EurJIC
European Journal of Inorganic Chemistry

Research Article
doi.org/10.1002/ejic.202300330

Chemistry Europe
European Chemical Societies Publishing

www.eurjic.org

Special Collection

Room-Temperature Synthesis of a Compositionally Complex Rare-Earth Carbonate Hydroxide and its Conversion into a Bixbyite-Type High-Entropy Sesquioxide

Jan Bernauer,[a] Maximillian Trapp,[b] Leonore Wiehl,[a] Hans-Joachim Kleebe,[b] and Emanuel Ionescu*[a, c]

In honor of the professional achievements of Prof. Rainer Streubel (University of Bonn, Germany)

In the present work, the solvent-deficient synthesis of the high-entropy rare-earth carbonate hydroxide $RE(CO_3)(OH)$ (RE = La, Ce, Pr, Nd, Sm, and Gd) and its thermal conversion into bixbyite-type sesquioxide RE_2O_3 are reported for the first time. The high-entropy rare earth carbonate hydroxide was prepared via mechanochemical reaction of the corresponding metal nitrate hydrates with ammonium hydrogen carbonate followed by the removal of the NH_4NO_3 by-product. Calcination of the carbonate hydroxide precursor in ambient atmosphere at temperatures in the range from 500 to 1000 °C led to the high-entropy rare earth sesquioxide which exhibited a bixbyite-type structure ($Ia\bar{3}$) independent of the calcination temperature. Transmission electron microscopy (TEM) investigation revealed the homogeneous distribution of all six rare earth cations in the high-entropy sesquioxide lattice, however, with some compositional variation between individual grains. The bixbyite-type structure may be considered as the result of heavy doping of the fluorite-type CeO_2 lattice with the other rare earth cations, which leads to a high concentration of oxygen vacancies, as revealed by electron diffraction and Raman spectroscopy data. The solvent-deficient synthesis method used in the present study is considered as a valuable, straightforward and easily upscalable method to synthesize compositionally complex oxide ceramics.

Introduction

Compositionally complex oxides, also called high-entropy (HE) oxides, emerged recently as highly interesting class of materials with novel and exciting physical and chemical properties.[1–9] They are characterized by a random distribution of near-equimolar fractions of five and more species on the cationic sublattice of the oxides. In various case studies, it has been shown exemplarily that the configurational entropy resulting from the random distribution of the cationic species within the crystal structure of the high-entropy oxides has a strong contribution to the formation of single-phase compositionally complex oxides.[1] The highly entropic cationic sublattice in compositionally complex oxides was shown to induce various exciting properties such as colossal dielectric constant,[10] unique electrochemical properties (Li ionic superconductivity, highly promising Li uptake/release behavior[11,12]), high-temperature stability, low thermal conductivity,[13,14] electrical,[15] magnetic[16] or catalytic properties.[9] Among the various classes of high-entropy oxides which have been prepared so far exhibiting e.g. rock salt, spinel, perovskite, or fluorite structure, rare earth (RE) sesquioxides represent an interesting category of high-entropy oxides due to the rich crystal chemistry of the binary $(RE)_2O_3$ compounds and their solid solutions.[17,18]

Recently, the synthesis and high-temperature evolution of the high-entropy sesquioxide $(Gd_{0.2}Tb_{0.2}Dy_{0.2}Ho_{0.2}Er_{0.2})_2O_3$ was reported.[19] This bixbyite-type was prepared using a polyvinyl alcohol (PVA)-based polymeric complex precursor which was calcined at temperatures beyond 1150 °C. It should be noted that all binary sesquioxides of the elements (Gd_2O_3, Tb_2O_3, Dy_2O_3, Ho_2O_3 and Er_2O_3) incorporated in the HE oxide possess the bixbyite-type structure at room temperature. Interestingly, the bixbyite-type sesquioxide showed an impressive phase stability up to 1500 °C, unlike the binary compounds such as Gd_2O_3 or Tb_2O_3, which undergo a bixbyite-to-monoclinic phase transition ($Ia\bar{3}\rightarrow C2/m$) at temperatures beyond 1250 °C (as for Gd) or coexist in multiple oxidation states and coordination geometries (as for Tb).[17,18] It was considered that the random distribution of the five rare earth elements on the cationic

[a] J. Bernauer, Dr. L. Wiehl, Dr. E. Ionescu
Institute for Materials Science
TU Darmstadt
Otto-Berndt-Str. 3, 64287 Darmstadt (Germany)

[b] M. Trapp, Prof. Dr. H.-J. Kleebe
Institute of Applied Geosciences
TU Darmstadt
Schnittspahnstr. 9, 64287 Darmstadt (Germany)

[c] Dr. E. Ionescu
Department Digitalization of Resources
Fraunhofer IWKS
Brentanostr. 2a, 63755 Darmstadt (Germany)
E-mail: emanuel.ionescu@iwks.fraunhofer.de

Special Collection Part of the celebratory collection for Rainer Streubel.

Research Article
doi.org/10.1002/ejic.202300330

sublattice is the main contribution for the full suppression of the bixbyite-to-monoclinic phase transformation.[19]

Other studies related to the synthesis of compositionally complex rare earth sesquioxides revealed that the preparative access (and notably the synthesis temperatures) strongly correlates with their crystal structure. For instance, Djenadic *et al.* prepared various three- and up to seven-component rare earth sesquioxides by means of nebulized spray pyrolysis and stated that the as-prepared single-phase sesquioxides possessed a fluorite-type ($Fm\bar{3}m$) structure which converts upon annealing at 1000 °C into the bixbyite-type structure ($Ia\bar{3}$).[20] The study concluded that the presence of Ce in the composition of the prepared sesquioxide was mandatory for the formation of high-entropy single-phase compounds and explained the low-temperature formation of the $Fm\bar{3}m$ structure as a direct consequence of Ce dominating the adopted structure of the prepared high-entropy sesquioxide.[20] Other studies showed however that the atmosphere during the calcination process has a crucial role whether a single-phase sesquioxide is generated, independently of the presence of Ce.[20b,c]

In a recent study, three sesquioxide compositions, i.e., $(La_{0.2}Sm_{0.2}Dy_{0.2}Er_{0.2}(RE)_{0.2})_2O_3$ (RE = Nd, Gd, Y) were shown to crystallize mainly with bixbyite-structure when prepared at a relatively low temperatures of 800 °C from a polymeric complex; whereas the same compositions showed mainly the monoclinic (*C2/m*) structure when prepared via splat quenching from the melt (from ca. 3000 °C) followed by extensive annealing at 800 °C.[21]

Here, we present the formation of a bixbyite-type six-component sesquioxide and its structural characterization. Unlike in the study from Tseng et al.,[19] the binary sesquioxides of the constituent rare earth elements possess trigonal structure ($P\bar{3}m1$), with the exception of Sm (monoclinic, *C2/m*) and Gd (bixbyite-type, $Ia\bar{3}$).[17,18] Thus, the formation of the bixbyite-type structure as sole phase in the resulting high-entropy sesquioxide is remarkable. Moreover, the preparative access to the high-entropy sesquioxide *via* the calcination of a high-entropy carbonate hydroxide precursor is described and discussed. The synthesis of the carbonate hydroxide precursor is being reported for the first time and was achieved via the so-called solvent-deficient synthesis method, which was successfully used for the synthesis of various nanocrystalline binary[22,23] and ternary oxides.[24,25]

Results and Discussion

Room-temperature synthesis of the compositionally complex carbonate hydroxide $RE(CO_3)(OH)$

The six-component sesquioxide investigated in the present study, i.e., RE_2O_3, was prepared starting from the corresponding rare earth nitrate hexahydrates which were ground together with ammonium hydrogen carbonate. This mechanochemical procedure has already been reported as a solvent-less or solvent-deficient, as the crystal water is released during the mechanochemical treatment, straight-forward and time efficient method to provide suitable precursors for nano-scaled binary and multinary metal oxides.[22] Typically, it is assumed that the ammonium hydrogencarbonate reacts with the metal nitrates in an anion exchange manner, thus a complex mixture of metal hydroxides and carbonates is anticipated as a product from this mechanochemical step. Subsequently, the precursor is calcinated and provides phase-pure and nanocrystalline oxides.[22]

In the present work, the product obtained from such a mechanochemical treatment of a metal nitrate hexahydrates mixture in the presence of ammonium hydrogen carbonate was investigated by means of X-ray diffraction as well as Raman spectroscopy. The XRD pattern of the as-prepared precursor (Figure 1a) indicates the presence of ammonium nitrate (*Pccn*) as well as additional reflections of a *Pnma* phase which was assigned to a high-entropy hydroxide carbonate, i.e., $(La_{0.167}Ce_{0.167}Pr_{0.167}Nd_{0.167}Sm_{0.167}Gd_{0.167})(CO_3)(OH)$. This is in agreement with previous work performed on the synthesis of the analogous monocation compounds $RE(CO_3)(OH)$, RE = La, Pr, Nd, Sm, Gd, which were reported to possess an orthorhombic (*Pnma*) structure.[27–29]

The as-prepared precursor was rinsed several times with cold water in order to remove the NH_4NO_3 and the resulting powder was investigated by XRD. The XRD pattern of the rinsed precursor is shown in Figure 1b and indicates the presence of the phase-pure *Pnma* high-entropy rare-earth carbonate hydroxide, $RE(CO_3)(OH)$.

The Raman spectrum of the synthesized precursor after the removal of NH_4NO_3 is presented in Figure 2 and agrees well with the XRD data. The broad signal at ca. 3460 cm^{-1} is attributed to the presence of the hydroxyl ions in the structure

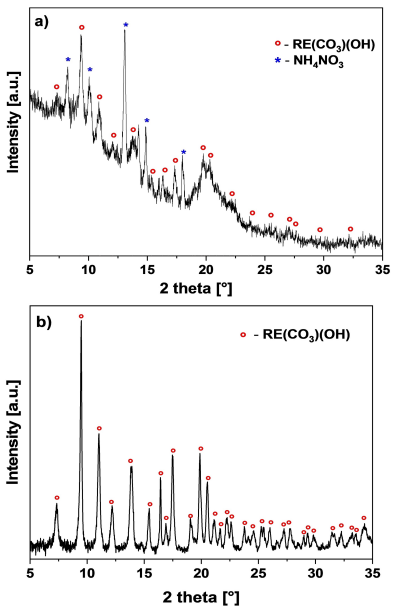

Figure 1. (a) XRD pattern of the mechanochemically *as-synthesized* precursor consisting of a compositionally complex hydroxide carbonate, $RE(CO_3)(OH)$ (*Pnma*), and NH_4NO_3 (*Pccn*) as secondary phase; (b) XRD pattern of the phase-pure $RE(CO_3)(OH)$ after removal of the NH_4NO_3 by-product.

Research Article
doi.org/10.1002/ejic.202300330

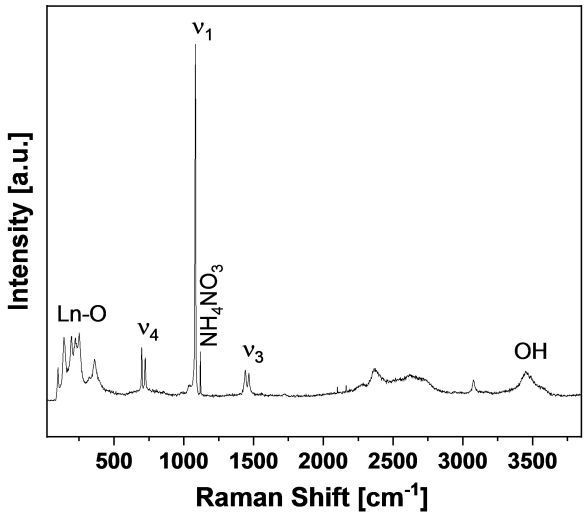

Figure 2. Raman spectrum of the compositionally complex carbonate hydroxide, $RE(CO_3)(OH)$ (*Pnma*).

of the precursor.[27,30] The high-intensity signal at 1083 cm^{-1} is assigned to the non-degenerated symmetric strech vibration of CO_3^{2-} (ν_1); whereas the two split signals at 1442/1464 cm^{-1} and 696/723 cm^{-1} are assigned to the doubly degenerated asymmetric stretch (ν_3) and the doubly degenerated asymmetric bend (ν_4) vibration, respectively.[31] The splitting of the ν_3 and ν_4 signals unambiguously shows the carbonate ions to be located/confined in the coordination sphere of the rare earth cations.[27] The low-intensity and very sharp signal at 1119 cm^{-1} indicates the presence of traces of NH_4NO_3.[32] The signals observed in the region below 500 cm^{-1} are attributed to vibrations of the RE–O bonds.[27,29]

The crystal water is being released during the mechanochemical treatment; however, its amount is not sufficient to provide full solvation of the nitrate salts and the ammonium hydrogen carbonate. For instance, considering the amounts used for the synthesis of the precursor, i.e., equimolar amounts of rare earth nitrate hexahydrates and a 1:3 molar ratio $RE(NO_3)_3$:NH_4HCO_3, the amount of the rare earth nitrates relative to the volume unity of the released crystal water corresponds to ca. 3.1 g $RE(NO_3)_3$/mL H_2O. This value exceeds the solubility product values of the rare earth nitrate (e.g., 0.63 g/mL as for $Ce(NO_3)_3$) by far[33,34]). Consequently, the process shown above is considered to occur via *gradual dissolution* of metal nitrates and NH_4HCO_3 in the released crystal water and their reaction leading to precipitation of the high-entropy rare-earth carbonate hydroxide and NH_4NO_3 as by-product. A similar process was demonstrated by Smith *et al.* for individual $M(NO)_3$-based systems.[22] However, for Ce^{3+}, Pr^{3+}, and Nd^{3+}, the respective hydroxide carbonates were observed as poorly crystallized main phases, along with, for example, carbonate or nitrate secondary phases; whereas for other rare earth nitrates, the mechanochemical treatment with NH_4HCO_3 led to mixture of carbonates, (hydro)oxides and carbonate hydroxides.[22] It is assumed that the reaction of the six rare-earth nitrates mixture with ammonium hydrogen carbonate is strongly simplified as compared to the individual rare earth nitrate compounds and possesses high selectivity with respect to the formation of the carbonate hydroxide compound. One may be tempted to correlate this fact to the configuration entropy of the resulting rare earth carbonate hydroxide. However, it is not clear yet whether and to which extent the configurational entropy of the resulting cationic sublattice may be responsible for the high selectivity of the reaction, especially the reaction occurs at room temperature.

The suggested reaction between the mixture of the lanthanide nitrate hexahydrates and the ammonium hydrogen carbonate[22] is given in the following:

$$1/6\ La(NO_3)_3 \cdot 6\ H_2O + 1/6\ Ce(NO_3)_3 \cdot 6\ H_2O + 1/6\ Pr(NO_3)_3 \cdot 6\ H_2O + 1/6\ Nd(NO_3)_3 \cdot 6\ H_2O + 1/6\ Sm(NO_3)_3 \cdot 6\ H_2O + 1/6\ Gd(NO_3)_3 \cdot 6\ H_2O + 3\ NH_4HCO_3 \rightarrow RE(CO_3)(OH) + 3\ NH_4NO_3 + 2\ CO_2 + 7\ H_2O,$$

with RE being equimolar composition of La, Ce, Pr, Nd, Sm and Gd.

The results obtained in the present work clearly show a simple and efficient synthetic procedure for the fabrication of a high-entropy rare earth carbonate hydroxide. To the best of our knowledge, this is the first report of a synthetic compositionally complex rare-earth-based carbonate hydroxide. Typically, metal hydroxide carbonates and in particular those of rare earths are prepared via various techniques, including precipitation method, sonochemical synthesis or hydrothermal synthesis, which all require the use of solvents as well as the exposure to high temperatures or rather long reaction times.[27,28,35] In contrast to that, the presented preparative route involves a very simple and quick room-temperature mechanochemical treatment of ca. 15–20 min.

The easy access to the compositionally complex hydroxide carbonate as single-phasic compound is in good agreement with the fact that there are numerous minerals belonging to the ancylite group, which is known to possess a large chemical variability, e.g., (i) ancylite-(Ce) – $(La,Ce)_{1.38}(Sr,Ca)_{0.62}(CO_3)_2(OH)_{1.38}$ 0.62 H_2O (*Pmcn*),[36] (ii) kozoite-(Nd) – $(Nd_{0.85}La_{0.61}Pr_{0.18}Sm_{0.14}Gd_{0.08}Eu_{0.05}Ca_{0.04}Y_{0.03}Ce_{0.01}Dy_{0.01})(CO_3)_2(OH)_2{\times}H_2O$ (*Pnma*),[37] or (iii) gysinite-(Nd) – $La_{0.16}Pb_{0.66}Nd_{1.18}(CO_3)_2(OH)\ H_2O$ (*Pnma*).[38]

Calcination of high-entropy $RE(CO_3)(OH)$ and its conversion into phase-pure high-entropy rare earth sesquioxide

The calcination of the as-prepared precursor was investigated by thermogravimetric analysis (TGA) combined with mass spectrometry (MS). The TGA curve and its first derivative are displayed in Figure 3a.

The as-prepared precursor exhibits a decomposition behavior with various mass loss steps, which have been assigned to the degradation of either NH_4NO_3 or of the high-entropy rare earth carbonate hydroxide, leading to a ceramic yield of ca. 37 wt.%. Typically, the decomposition of NH_4NO_3 follows a rather complex pattern and leads to the release of various

Research Article
doi.org/10.1002/ejic.202300330

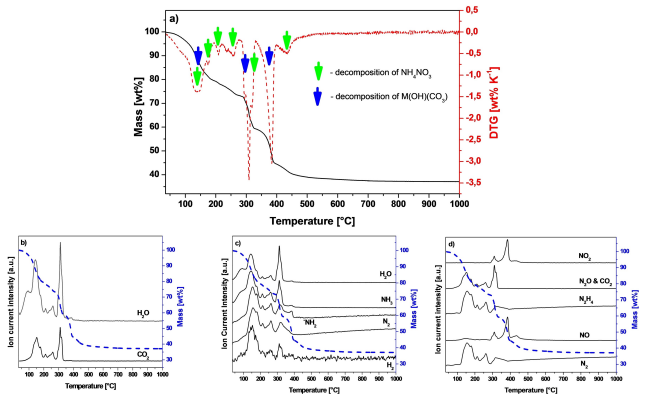

Figure 3. (a) TGA curve (black) and its first derivate (red) for the calcination process of the synthesized precursor (green and blue arrow indicate decomposition steps of NH_4NO_3 and of the high-entropy rare earth carbonate hydroxide, respectively); (b)–(d) QMID (quasi multiple ion detection) current curves for various gaseous species released during the calcination process.

species such as NH_3, N_2, H_2, N_2O, NO, NO_2 and H_2O (Figure 3c and 3d);[39,40] whereas, the decomposition of the high-entropy rare earth carbonate hydroxide mainly occurs via release of CO_2 and H_2O (Figure 3b), as reported for other rare earth carbonate hydroxides.[27]

The decomposition process of the precursor can be described in a simplified manner by following reactions;[27,40] with the only exception of HNO_3, all other reaction products were detected via *in situ* mass spectrometry:

$$NH_4NO_3 \rightarrow N_2O + 2\ H_2O$$

$$NH_4NO_3 \rightarrow N_2 + 2\ H_2O + 0.5\ O_2$$

$$5\ NH_4NO_3 \rightarrow 2\ HNO_3 + 4\ N_2 + 9\ H_2O$$

$$NH_4NO_3 \rightarrow NH_3 + HNO_3$$

$$HNO_3 \rightarrow NO_2 + H_2O$$

$$NH_3 \rightarrow N_2H_4 + H_2$$

$$2\ RE(CO_3)(OH) \rightarrow RE_2(CO_3)O_2 + CO_2 + H_2O$$

$$RE_2(CO_3)O_2 \rightarrow RE_2O_3 + CO_2$$

Based on the results obtained from the thermogravimetry analysis, the precursor was calcined in air at three different temperatures, 500 °C, 600 °C and 1000 °C. Subsequently, the obtained powders were investigated by Raman spectroscopy, X-ray diffraction and transmission electron microscopy.

As shown in Figure 4, the Raman spectra of the samples obtained upon calcination of the precursor at 500 and 1000 °C resemble each other to a large extent. For both spectra, signals indicating the presence of the bixbyite-type structure ($Ia\bar{3}$) were identified. Typically, the $Ia\bar{3}$ space group possesses 22 Raman active modes, i.e., 4 A_g, 4 E_g and 14 F_g; however, only some of them were observed experimentally.[41–43] The Raman spectra of

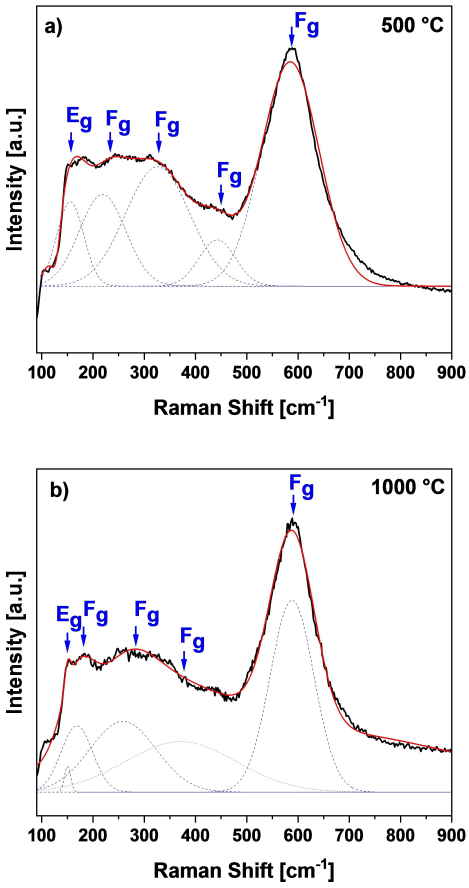

Figure 4. Raman spectra of the oxidic products obtained via calcination of the precursor at (a) 500 °C and (b) 1000 °C. Both spectra show the signature of the bixbyite-type structure ($Ia\bar{3}$) of the high-entropy rare earth sesquioxide. Moreover, a significant amount of oxygen vacancies in the structure is assumed, based on the strong mode at ca. 580 cm^{-1}.

the two investigated oxide samples possess similar $Ia\bar{3}$-related signature, one E_g and four F_g modes, as depicted in Figure 4.

The strong mode positioned at ca. 580 cm^{-1}, which was observed in both spectra taken from the samples calcined at 500 and 1000 °C, should be emphasized, as this mode has been correlated with the reduction or the extrinsic (heavy) doping of ceria with rare earth elements with oxidation state 3+.[44] Employing the Kröger-Vink notation for the incorporation of for example samarium(III)oxide into the ceria crystal lattice, it can be shown that oxygen vacancies are formed to maintain charge neutrality:

$$Sm_2O_3 \xrightarrow{CeO_2} 2Sm_{Ce}^{\bullet} + 3O_O^{x} + V_O^{//} \quad (1)$$

Heavy doping of CeO_2 with rare earth sesquioxide has been shown to induce a strong increase of the full width at half maximum (FWHM) as well as a splitting of the fluorite-structure-related F_{2g} mode.[44] These effects have been considered being a consequence of phonon scattering at oxygen vacancies, as well as of doping-related presence of non-equivalent RE–O bonds in the crystal lattice.[44,45] This is not seen in the present work, as the Raman signature of all prepared sesquioxide samples indicated a sole $Ia\bar{3}$ bixbyite structure. However, the mode at

Research Article
doi.org/10.1002/ejic.202300330

580 cm^{-1} has been observed in heavily-doped ceria and even in nanocrystalline ceria and was assigned to oxygen vacancies in the lattice[44,46–48] or to the formation of oxygen vacancy-dopant defect complexes.[49] The latter would induce oxygen vacancies ordering in the lattice, as reported for instance by Ou et al.[50] This possibility will be discussed below within the context of the obtained electron diffraction data (compare Figure 7). In summary, based on the Raman data, it can be concluded that the calcination of the precursor results in the formation of the bixbyite-type structure already at 500 °C. Moreover, it is shown that the bixbyite structure remains stable upon heating to 1000 °C.

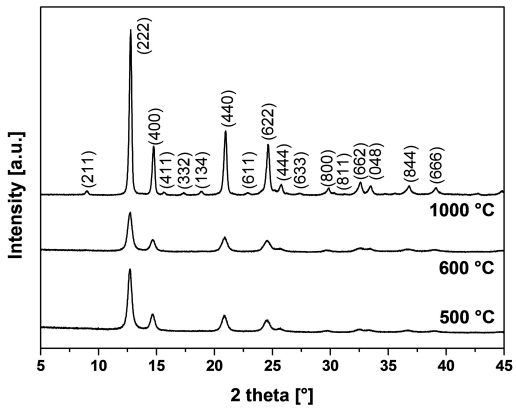

Figure 5. X-ray diffraction patterns of the samples calcinated at 500 °C, 600 °C and 1000 °C.

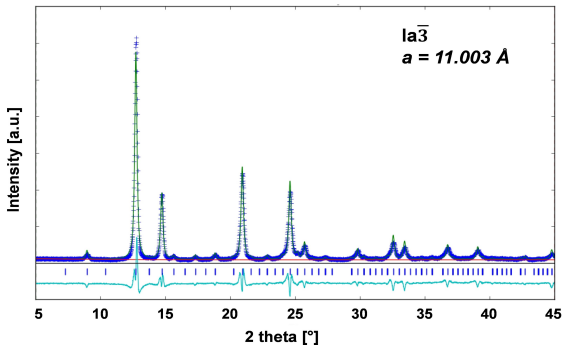

Figure 6. Rietveld refinement of the sample prepared via calcination at 1000 °C.

The samples were additionally studied by means of XRD. The corresponding XRD patterns are shown in Figure 5. The sample prepared at 1000 °C exhibits the presence of the Ia$\bar{3}$ structure as a sole phase, as expected, and thus is in agreement with the Raman spectroscopy data. The XRD data for the samples prepared via calcination at 500 and 600 °C can be discussed in two ways. Firstly, one can assume that they may indicate the presence of a fluorite-type *Fm*$\bar{3}$*m* structure (which possesses a higher symmetry than the bixbyite-type structure with half of the lattice parameter). This is supported by the absence of the (411), (332), (134), (611) or (633) in the patterns of the samples prepared at 500 and 600 °C. Secondly, a bixbyite-type structure can be assumed in both samples with the absence of the superstructure reflections as a consequence of the poor(er) crystallinity. The Raman spectroscopy data clearly indicates the presence of the bixbyite-type phase in all studied samples, independent of the calcination temperature; please note that the *Fm*$\bar{3}$*m* phase of the oxide would be characterized by only one F_{2g} mode, in the Raman spectrum, at ca. 450 cm^{-1},[51] in contrast to those observed and shown in Figure 4, which are typical for Ia$\bar{3}$. It is thus concluded that all three samples possess the bixbyite-type structure and that the absence of the superstructure reflections in the samples calcined at 500 and 600 °C is related to their poor(er) crystallinity (Figure 5).

Furthermore, Rietveld refinement was applied to the XRD pattern of the sample prepared at 1000 °C (see Figure 6 and Table 1). As a result, the bixbyite-type structure was confirmed, with a lattice parameter $a = 11.003$ Å and an average crystallite size of 25 nm.

Figure 7 depicts a BF-TEM micrograph of an individual particle of the high-entropy rare earth sesquioxide calcined at 1000 °C, and its corresponding selected area electron diffraction (SAED) image. The electron diffraction pattern clearly reveals the predominant single-crystalline nature of the particle, although it is rather inhomogeneously crystallized and possibly

Table 1. Refinement results for $(La_{0.167}Ce_{0.167}Pr_{0.167}Nd_{0.167}Sm_{0.167}Gd_{0.167})_2O_3$. Space group Ia$\bar{3}$ (No. 206), a = 11.003(2) Å, agreement factor wR = 17%. Nd was used as replacement for the six rare earth (RE) elements because its ionic radius (for coordination number 6) of 98 pm fits very well to the mean value < r > = 98.5 () of the ionic radii of the six RE elements in the sample. However, the mean scattering power of the atomic mixture in the compositionally complex structure at the two cation lattice sites is not perfectly represented by Nd, as indicated by the occupancy factors smaller than unity, which must not be interpreted as missing atoms but rather in terms of atomic scattering power slightly different from that of Nd.

	x	y	z	occupancy
RE1	0.25000	0.25000	0.25000	0.903(27)
RE2	0.4668(1)	0.00000	0.25000	0.869(19)
O1	0.3867(22)	0.1510(18)	0.3781(28)	1.000
Atom (site symmetry)			RE–O distance	
Nd1 (-3)			2.331(25) Å (6×)	
Nd2 (2)			2.262(25) Å (2×)	
			2.417(25) Å (2×)	
			2.489(26) Å (2×)	

Research Article
doi.org/10.1002/ejic.202300330

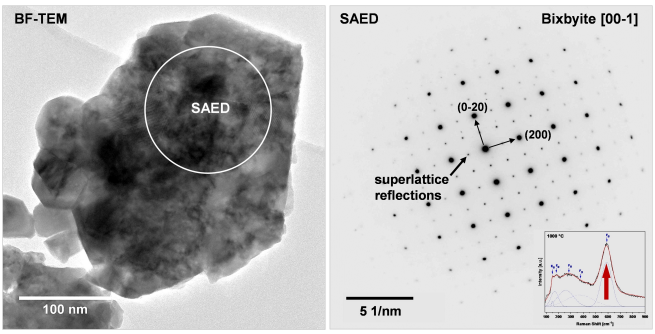

Figure 7. BF-TEM image of the sesquioxide powder sample calcined at 1000 °C and a corresponding SAED image of the bixbyite structure in [00-1] orientation. The main part of the investigated particle is indeed single crystalline, as revealed by the SAED pattern. Nevertheless, the BF contrast also indicates a rather inhomogeneously crystallized, possibly defect-rich grain agglomerated or intergrown with smaller crystallites. Superlattice reflections are clearly visible in the electron-diffraction pattern (marked by arrow), which have been correlated with oxygen vacancy ordering in the fluorite-type structure, leading to the observed bixbyite-type structure with doubled lattice parameter. The inset in the lower right of the SAED pattern reveals the Raman spectrum of this sample, highlighting the presence of oxygen vacancies (see also Figure 4).

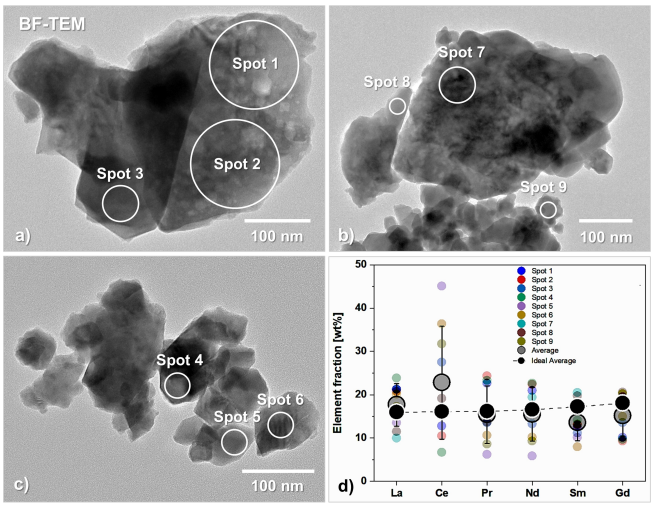

Figure 8. BF-TEM images a)–c) depicting various high-entropy sesquioxide powder particles calcined at 1000 °C. The white circles indicate the spots at which EDS measurements were performed. In d), the element distribution fraction of the rare earth elements is given, based on the nine EDS measurements recorded from the indicated grains. Colored dots correspond to the individual measured weight fractions of the elements. Grayish dots indicate the average elemental contents based on the individual measurements (bars indicate standard deviation). The black dots represent the target weight fractions of the six rare earth elements. According to the EDS measurements and to the separately determined oxygen content of 15.84 wt% via hot-gas combustion analysis, the estimated average composition of the bixbyite-type high-entropy sesquioxide corresponds to $\left(La^{III}_{0.18}Ce^{IV}_{0.23}Pr^{IV}_{0.16}Nd^{III}_{0.15}Sm^{III}_{0.13}Gd^{III}_{0.15}\right)_2O_{3.39}$.

defect-rich as revealed by the non-uniform contrast in the BF image. Furthermore, Moiré patterns and traces of grain boundaries, despite being hardly visible, indicate the presence of small adjacent grains forming an agglomeration or intergrowth typical for this sample. It should be noted that the locally varying thickness as well as regions tilted from the perfect zone axis condition also contribute to the observed contrast variations. In the SAED image, all reflections were found to be perfectly consistent with bixbyite space group $Ia\bar{3}$ and a lattice parameter of $a = 11$ Å, which is in excellent agreement with the Rietveld refinement data given in Figure 6. Only the strong reflections might be interpreted by a fluorite-type structure, showing half the lattice parameter. The weaker, yet clearly visible reflections, which are marked by arrow in the SAED pattern in Figure 7, represent superlattice (SL) reflections with respect to the fluorite-type. Since those SL reflections occur precisely in the middle of the strong reflections, a doubling of the unit cell as compared to that of fluorite can be assumed. This reflects indeed the structural relationship fluorite-bixbyite, with fluorite which may be converted into bixbyite (with doubled lattice parameters as compared to those of fluorite) upon replacing 1/8 of anions by constitutional vacancies.[52,53]

The occurrence of oxygen vacancies in heavily doped ceria-based materials has been indeed reported.[44,46–48] Moreover, the ordering of such oxygen vacancies was also reported, e.g., by Ou et al.[50,52,53] Taking the Raman data of the sesquioxide powder samples calcined at 500 and 1000 °C (see Figure 4) into account, it is concluded that the presence of superlattice reflections in this system is directly related to an ordering process of oxygen vacancies within the fluorite, leading to the bixbyite crystal structure with double lattice parameter.

Figure 8a shows BF-TEM micrographs of various grains of the sample prepared at 1000 °C. The small white circles indicate spots on nine different grains which were analyzed by means of EDS with respect to the composition of the rare earth elements in the high-entropy sesquioxide. The obtained data were used in combination with the information on the overall oxygen content, which was separately determined by means of hot-gas combustion (see Experimental Procedure), to evaluate the elemental compositions of the nine grains; the results are plotted in Figure 8d and indicate that the elemental content of the individual rare earths fluctuates to some extent among the grains. Especially Ce shows notably large variation of its local content (colored dots in Figure 8d) and, additionally, an average value (gray dots) being larger than the corresponding equimolar composition (black dots).

All other rare earth elements show contents closer to the equimolar composition as well as markedly less variation. According to the individual elemental contents, the bixbyite-type oxide prepared at 1000 °C has an overall composition of $(La_{0.18}Ce_{0.23}Pr_{0.16}Nd_{0.15}Sm_{0.13}Gd_{0.15})_2O_{3+x}$. Elemental analysis via hot-gas combustion revealed an oxygen content in the high-entropy sesquioxide of 15.84 wt% which corresponds to a value for x being 0.39, thus indicating that the rare earths are present in both oxidation states, 3+ and 4+. Note that for the situation of having all six rare earth elements being present with oxidation state 3+, an oxygen content of 14.23 wt% would be expected. Moreover, for the sake of electroneutrality, both Ce and Pr in the bixbyite-type structure are expected to have exclusively the oxidation state 4+, thus the composition of the high-entropy sample calcined at 1000 °C can be estimated as $\left(La^{III}_{0.18}Ce^{IV}_{0.23}Pr^{IV}_{0.16}Nd^{III}_{0.15}Sm^{III}_{0.13}Gd^{III}_{0.15}\right)_2O_{3.39}$. This result is in good

Research Article
doi.org/10.1002/ejic.202300330

agreement with previous studies related to high-entropy rare earth sesquioxides containing Ce and Pr.[20,47] However, it should be noted that the oxidation states of the rare earth elements of the bixbyite-type sesquioxide studied in the present work can only be estimated based on the chemical composition; XPS and XANES/EXAFS data should be recorded for further substantiation.

In Figure 9, a DF-STEM micrograph of the sesquioxide prepared at 1000 °C as well as the corresponding EDS maps are given, showing the local distribution of oxygen and the six rare-earth elements present in an individual grain.

The inhomogeneous contrast in the DF-STEM image indicates thickness variations, which also imply the presence of pores, surface steps or the presence of small agglomerated crystallites, similar to the findings in Figure 7a. The intensities of all rare earth elements as well as oxygen follow the shape and thickness of the grains, depicting a homogenous elemental distribution within the crystal structure. The Ce-rich regions on the right and at the bottom are separate grains with a higher elemental content of this species as compared to the large main crystal in the middle. Therefore, this observation is not only consistent with the results from the EDS point measurements (Figure 8) but also illustrates them well within the EDS maps. In summary, based on the structural and chemical data obtained from the samples investigated, it is concluded that these indeed represent a single-phase crystalline material with a highly entropic cationic sublattice.

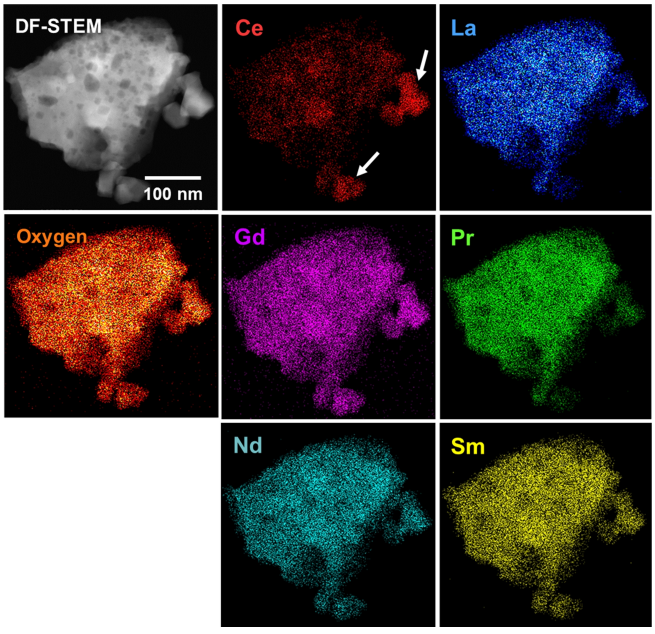

Figure 9. DF-STEM micrograph of the bixbyite-type high-entropy sesquioxide sample prepared at 1000 °C and corresponding EDS maps showing the distribution of oxygen and of the six rare-earth elements within an individual grain. Oxygen as well as all rare earth elements are found to be rather homogeneously distributed. It should be noted that the Ce-rich regions on the right and at the bottom are separated grains (marked by arrows) and therefore depict an elemental variation among different grains instead of variations within an individual one.

Conclusions

In the present work, a room-temperature, straight forward synthesis method for an orthorhombic high-entropy rare earth carbonate hydroxide is presented for the first time. Furthermore, its calcination in air is shown to deliver a phase-pure bixbyite-type high-entropy rare-earth sesquioxide at a temperature as low as 500 °C, which was structurally characterized by means of XRD, Raman spectroscopy and TEM imaging. The bixbyite structure of the prepared high-entropy sesquioxide possesses a rather good homogeneity concerning elemental variations on lattice sites, with some content fluctuations, in particular, of the high-oxidation-state elements, Ce and Pr. This synthesis method employed in the present study can be utilized also for accessing other high-entropy oxides with various elemental compositions (transition metals, rare earths etc.) as well as different base structures (e.g., perovskite or spinel).

Experimental Section

Materials Synthesis: Equimolar quantities of the hydrated nitrate salts ($RE(NO_3)_3 \cdot 6\ H_2O$) of La, Ce, Pr, Nd, Sm and Gd ($RE(NO_3)_3 \cdot 6\ H_2O$, Sigma-Aldrich, 99.9%) were ground in a mortar together with ammonium hydrogen carbonate (NH_4HCO_3, Sigma-Aldrich, $\geq$99%) for 15 minutes. The metal nitrate to bicarbonate ratio was set to 1:3. During the grinding, a bubbling slurry was formed. After the complete 15 minutes of grinding, a paste-like precursor was obtained which was then dried at 80 °C for several days. Subsequently, the dry powder was rinsed several times with cold water in order to remove the NH_4NO_3 by-product, dried at 80 °C and calcinated in ambient atmosphere at different temperatures (i.e., 500 °C, 600 °C and 1000 °C).

Samples Characterization: X-ray diffraction (XRD) measurements were performed on a STOE X-Ray diffractometer utilizing Mo-K_α – radiation ($\lambda = 0.7093$ Å). Rietveld refinements were performed using the program GSAS-II.[26] The thermogravimetric analysis was carried out on a STA449C Jupiter (Netzsch Gerätebau GmbH) thermal analyzer (TG/DTA), in situ coupled with a quadrupole mass analyzer QMS 403C Aëolos (Netzsch Gerätebau GmbH) and a FTIR-Spectrometer Tensor 27 (Bruker Optik GmbH) with a „Y-head"-connection. The samples were annealed under synthetic air (20% oxygen, 80% nitrogen) from RT to 1000 °C. Raman spectroscopic measurements were done with a Horiba HR800 micro-Raman spectrometer (Horiba Jobin Yvon, Bensheim, Germany) equipped with a green laser (irradiation wavelength 514.5 nm). The excitation line has its own interference filter (to filter out the plasma emission) and a Raman notch filter (for laser light rejection). The elemental analysis was carried out on a LECO TC-436 analyzer to determine the contents of N (0.5 ppm – 0.5% with 0.25 ppm or 0.5% RSD, as thermal heat capacity) and O (0.5 ppm – 0.1% with 0.25 ppm or 0.5% RSD, as CO_2 IR absorption). Transmission electron microscopy (TEM) studies were performed on the powder sample calcined at 1000 °C, which was mildly coated with carbon to minimize electrostatic charging under the incident electron beam. Bright-field TEM (BF-TEM) as well as selected area electron diffraction (SAED) and, in addition, dark-field scanning TEM (DF-STEM) in conjunction with energy-dispersive X-ray spectroscopy (EDS) mapping for local chemical analysis, were recorded with a JEOL JEM-2100F (JEOL, Tokyo, Japan) microscope operating at 200 kV, being equipped with a CCD camera and a JEOL Be double-tilt holder for sample orientation, while EDS spectra were acquired using an Oxford

XMAX 80 detector (Oxford Instruments NanoAnalysis, Wiesbaden, Germany).

Acknowledgements

E. I. acknowledges the German Research Foundation (DFG, Bonn, Germany) for financial support within the Heisenberg Program (IO 64/14-1). Dr. Marc Widenmeyer is gratefully acknowledged for recording the XRD pattern of the precursors and Ms. Claudia Fasel for performing the TGA/MS experiments. Open Access funding enabled and organized by Projekt DEAL.

Conflict of Interests

The authors declare no conflict of interest.

Data Availability Statement

The data that support the findings of this study are available from the corresponding author upon reasonable request.

Keywords: bixbyite-type structure · ceramics · high-entropy oxides · solvent-deficient synthesis · rare earths

[1] C. M. Rost, E. Sachet, T. Borman, A. Moballegh, E. C. Dickey, D. Hou, J. L. Jones, S. Curtarolo, J.-P. Maria, *Nat. Commun.* **2015**, *6*, 8485.
[2] A. Sarkar, Q. Wang, A. Schiele, M. R. Chellali, S. S. Bhattacharya, D. Wang, T. Brezesinski, H, Hahn, L. Velasco, B. Breitung, *Adv. Mater.* **2019**, *31(26)*, e1806236.
[3] S. J. McCormack, A. Navrotsky, *Acta Mater.* **2021**, *202*, 1–21.
[4] B. L. Musicó, D. Gilbert, T. Z. Ward, K. Page, E. George, J. Yan, D. Mandros, V. Keppens, *APL Mater.* **2020**, *8(4)*, 040912.
[5] P. B. Meisenheimer, J. T. Heron, *MRS Advances* **2020**, *5(64)*, 3419–3436.
[6] C. Oses, C. Toher, S. Curtarolo, *Nat. Rev. Mater.* **2020**, *5(4)*, 295–309.
[7] R.-Z. Zhang, M. J. Reece, *J. Mater. Chem. A* **2019**, *7(39)*, 22148–22162.
[8] S. H. Albedwawi, A. AlJaberi, G. N. Haidemenopoulos, K. Polychronopoulou, *Mater. Des.* **2021**, *202*, 109534.
[9] Y. Sun, S. Dai, *Sci. Adv.* **2021**, *7(20)*, eabg1600.
[10] D. Bérardan, S. Franger, D. Dragoe, A. K. Meena, N. Dragoe, *Phys. Status Solidi RRL* **2016**, *10(4)*, 328–333.
[11] A. Sarkar, L. Velasco, D. Wang, Q. Wang, G. Talasila, L. de Biasi, C. Kübel, T. Brezesinski, S. S. Bhattacharya, H. Hahn, B. Breitung, *Nat. Commun.* **2018**, *9(1)*, 3400.
[12] D. Bérardan, S. Franger, A. K. Meena, N. Dragoe, *J. Mater. Chem. A.* **2016**, *4(24)*, 9536–9541.
[13] F. Li, L. Zhou, J.-X. Liu, Y. Liang, G.-J. Zhang, *J. Adv. Ceram.* **2019**, *8(4)*, 576–582.
[14] J. L. Braun, C. M. Rost, M. Lim, A. Giri, D. H. Olson, G. N. Kotsonis, G. Stan, D. W. Brenner, J. P. Maris, P. E. Hopkins, *Adv. Mater.* **2018**, *30(51)*, e1805004.
[15] H. Li, Y. Zhou, Z. Liang, H. Ning, X. Fu, Z. Xu, T. Qiu, W. Xu, R. Yao, J. Peng, *Coating* **2021**, *11(6)*, 628.
[16] R. Witte, A. Sarkar, R. Kruk, B. Eggert, R. A. Brand, H. Wende, H. Hahn, *Phys. Rev. Mater.* **2019**, *3(3)*, 034406.
[17] Y. Zhang, I.-H. Jung, *Calphad* **2017**, *58*, 169–203.
[18] M. Zinkevich, *Prog. Mater. Sci.* **2007**, *52(4)*, 597–647.
[19] K.-P. Tseng, Q. Yang, S. J. McCormack, W. M. Kriven, *J. Am. Ceram. Soc.* **2020**, *103(1)*, 569–576.
[20] a) R. Djenadic, A. Sarkar, O. Clemens, C. Loho, M. Botros, V. S. K. Chakravadhanula, C. Kübel, S. S. Bhattacharya, A. S. Gandhi, H. Hahn, *Mater. Res. Lett.* **2017**, *5(2)*, 102–109; b) L. Velasco, J. S. Castillo, M. V. Kante, J. J. Olaya, P. Friederich, H. Hahn, *Adv. Mater.* **2021**, *33(43)*, 2102301; c) M. Kumbhakar, A. Khandelwal, S. K. Jha, M. V. Kante, P. Keßler, U. Lemmer, H. Hahn, J. Aghassi-Haghmann, A. Colsmann, B. Breitung, *Adv. Energy Mater.* **2023**, *13(24)*, 2204337.
[21] S. V. Ushakov, S. Hayun, W. Gong, A. Navrotsky, *Materials* **2020**, *13(14)*, 3141.
[22] S. J. Smith, B. Huang, S. Liu, Q. Liu, R. E. Olsen, J. Boerio-Goates, B. F. Woodfield, *Nanoscale* **2015**, *7(1)*, 144–156.
[23] R. M. Kore, B. J. Lokhande, *Electrochim. Acta* **2017**, *245*, 780–790.
[24] K. N. Nithyayini, M. N. K. Harish, K. L. Nagashree, *Electrochim. Acta* **2019**, *317*, 701–710.
[25] S. Zeljković, T. Ivas, H. Maruyama, J. C. Nino, *Ceram. Int.* **2019**, *45(16)*, 19793–19798.
[26] B. H. Toby, R. B. von Dreele, *J. Appl. Crystallogr.* **2013**, *46(2)*, 544–549.
[27] M. Hämmer, H. A. Höppe, *Z. Naturforsch. B* **2019**, *74(1)*, 59–70.
[28] A. M. Kaczmarek, K. van Hecke, R. van Deun, *Chem. Soc. Rev.* **2015**, *44(8)*, 2032–2059.
[29] C. S. Riccardi, R. C. Lima, M. L. dos Santos, P. R. Bueno, J. A. Varela, E. Longo, *Solid State Ionics* **2009**, *180(2–3)*, 288–291.
[30] P. Jeevanandam, Y. Koltypin, O. Palchik, A. Gedanken, *J. Mater. Chem.* **2001**, *11(3)*, 869–873.
[31] A. M. Kaczmarek, L. Miermans, R. van Deun, *Dalton Trans.* **2013**, *42(13)*, 4639–4649.
[32] H. C. Tang, B. H. Torrie, *J. Phys. Chem. Solids* **1977**, *38(2)*, 125–138.
[33] L. L. Quill, R. F. Robey, *J. Am. Chem. Soc.* **1937**, *59(12)*, 2591–2595.
[34] S. Siekierski, T. Mioduski, M. Salomon, *IUPAC Solubility Data Series: Scandium, yttrium, lanthanum, and lanthanide nitrates*, London, Pergamon Press; **1983**.
[35] A. M. Szucs, A. Stavropoulou, C. O'Donnell, S. Davis, J. D. Rodriguez-Blanco, *Cryst. Growth Des.* **2021**, *21(1)*, 512–527.
[36] A. Dal Negro, G. Rossi, V. Tazzoli, *Am. Mineral.* **1975**, *60 (3–4)*, 280–284.
[37] R. Miyawaki, S. Matsubara, K. Yokoyama, K. Takeuchi, Y. Terada, I. Nakai, *Am. Mineral.* **2000**, *85(7–8)*, 1076–1081.
[38] W.-J. Feng, G.-P. Zhou, Z.-B. Liu, Y. Xu, *Acta Crystallogr. Sect. E* **2007**, *63(9)*, i174.
[39] Y. Wang, X. Song, F. Li, *ACS Omega* **2019**, *4(1)*, 214–225.
[40] V. Babrauskas, D. Leggett, *Fire Mater.* **2020**, *44(2)*, 250–268.
[41] M. V. Abrashev, N. D. Todorov, J. Geshev, *J. Appl. Phys.* **2014**, *116(10)*, 103508.
[42] Y. Repelin, C. Proust, E. Husson, J. M. Beny, *J. Solid State Chem.* **1995**, *118(1)*, 163–169.
[43] N. D. Todorov, M. V. Abrashev, V. Marinova, M. Kadiyski, L. Dimowa, E. Faulques, *Phys. Rev. B* **2013**, *87(10)*, 104301.
[44] R. Schmitt, A. Nenning, O. Kraynis, R. Korobko, A. I. Frenkel, I. Lubomirsky, S. M. Haile, J. L. M. Rupp, *Chem. Soc. Rev.* **2020**, *49(2)*, 554–592.
[45] R. Korobko, S. K. Kim, S. Kim, S. R. Cohen, E. Wachtel, I. Lubomirsky, *Adv. Funct. Mater.* **2013**, *23(48)*, 6076–6081.
[46] C. Schilling, A. Hofmann, C. Hess, M. V. Ganduglia-Pirovano, *J. Phys. Chem. C.* **2017**, *121(38)*, 20834–20849.
[47] A. Sarkar, B. Eggert, L. Velasco, X. Mu, J. Lill, K. Ollefs, S. S. Battacharya, H. Wende, R. Kruk, R. A. Brand, H. Hahn, *APL Mater.* **2020**, *8(5)*, 51111.
[48] A. Banerji, V. Grover, V. Sathe, S. K. Deb, A. K. Tyagi, *Solid State Commun.* **2009**, *149(39–40)*, 1689–1692.
[49] A. Nakajima, A. Yoshihara, M. Ishigame, *Phys. Rev. B: Condens. Matter Mater. Phys.* **1994**, *50(18)*, 13297–13307.
[50] D. R. Ou, T. Mori, F. Ye, T. Kobayashi, J. Zou, G. Auchterlonie, J. Drennan, *Appl. Phys. Lett.* **2006**, *89(17)*, 171911.
[51] J. Cui, G. A. Hope, *J. Spectr.* **2015**, 940172.
[52] D. J. M. Bevan, R. L. Martin, *J. Solid State Chem.* **2008**, *181*, 2250–2259.
[53] D. Lee, X. Gao, L. Sun, Y. Jee, J. Poplawsky, T. O. Farmer, L. Fan, E.-J. Guo, Q. Lu, W. T. Heller, Y. Choi, D. Haskel, M. R. Fitzsimmons, M. F. Chisholm, K. Huang, B. Yildiz, H. N. Lee, *Nat. Commun.* **2020**, *11*, 1371.

Manuscript received: May 30, 2023
Revised manuscript received: November 21, 2023
Accepted manuscript online: November 22, 2023
Version of record online: December 7, 2023